Surface & Coatings Technology 480 (2024) 130564

Contents lists available at ScienceDirect

Surface & Coatings Technology

journal homepage: www.elsevier.com/locate/surfcoat

Full length article

Comparison of surface modification and corrosion resistance of Ti6Al4V alloy using matcha tea extract-based silver and copper oxide nanoparticles

Gizem Karabulut [a,*], Nuray Beköz Üllen [a], Selcan Karakuş [b], Mustafa Ersoy [a,c]

[a] Istanbul University-Cerrahpaşa, Faculty of Engineering, Department of Metallurgical and Materials Engineering, Istanbul, Turkiye
[b] Istanbul University-Cerrahpaşa, Faculty of Engineering, Department of Chemistry, Istanbul, Turkiye
[c] VALEO Automotive Industry and Trade Inc., Istanbul, Turkiye

ARTICLE INFO

Keywords:
Ti6Al4V alloy
Silver nanoparticles
Copper oxide nanoparticles
Surface modification
Corrosion resistance

ABSTRACT

In this study, our aim was to investigate the application of green-synthesized silver nanoparticles (Ag NPs) and copper oxide nanoparticles (CuO NPs) for surface modification, specifically focusing on their influence on the corrosion properties of Ti6Al4V alloy. The green NPs were thoroughly characterized, and their role in enhancing the anticorrosive performance of Ti6Al4V was carefully evaluated. Various coating methods and drying temperatures were utilized to coat Ti6Al4V samples with the NPs, aiming to assess their impact on corrosion resistance. The electrochemical corrosion behavior was examined through electrochemical polarization tests in Ringer's bio-liquid. The study underscored the significant impact of coating type, coating method, and drying temperature (25 °C and 60 °C) in achieving favorable anticorrosive performance. Notably, samples oven-dried at both temperatures and coated with Ag NPs and CuO NPs using spray coating demonstrated the most effective substrate protection, achieving protection efficiencies of 97.37 % and 90.56 %, respectively. This outcome can be attributed to the unique spherical and homogeneously dispersed particulate structure of the NPs, effectively reducing microporosity. In summary, the combination of increased surface area and reduced microporosity resulting from the surface properties of the NPs underscores the potential of well-designed surface modification approaches in advancing the development of titanium-based implants for biomedical applications.

1. Introduction

The Ti6Al4V alloy exhibits excellent corrosion resistance, good mechanical strength, and biocompatibility within the human environment, making it a widely used material in dental, endovascular, and orthopedic surgeries [1]. In comparison to Co-Cr alloys and stainless steels, the Ti6Al4V alloy demonstrates higher biocompatibility, primarily attributed to its surface properties. However, the prolonged presence of metal-based implants in the host body carries the risk of corrosion formation, potentially diminishing the implants' performance over time and leading increased inflammatory responses. The outstanding performance of Ti6Al4V alloy as an implant materials in the short, medium, and long term can be attributed to the presence of a natural TiO_2 passive oxide layer [2,3]. The oxide layer contributes to both favorable biocompatibility and corrosion resistance. When Ti6Al4V implants come into contact with bone tissue, a series of biological reactions take place, emphasizing the critical role of the implant surface at the initial point of contact critical [4]. While the Ti6Al4V alloy is well-tolerated, its passive oxide layer is considered bioinert due to a lack of interaction with surrounding tissues or cells. Consequently, a crucial strategy for addressing the corrosion issue is to design nano-scale surface modifications for Ti6Al4V implants with long-term effective anti-corrosion properties. Enhancing corrosion resistance is of utmost importance for metallic implants. In recent years, there has been significant research interest in nanostructured surface coatings as a cost-effective, environmentally friendly, and promising approach to enhance corrosion resistance in various medical applications. With the growing life expectancy, there is an increasing demand for longer lifespan of metallic implants. This is particularly crucial in load-bearing applications, such as orthopedic replacements, where high corrosion resistance is essential to prolong implant life and minimize the need for revision surgeries [5–9]. Significant attention has been directed towards recognizing the vital role of implant surface modification to the overall success of implants. The coating product formed on the surface not only shapes the structure of the implant surface but also profoundly influences the body's response to it. Consequently, surface modification stands out as the most effective

* Corresponding author at: Istanbul University-Cerrahpaşa, Faculty of Engineering, Department of Metallurgical and Materials Engineering, İstanbul, Turkiye.
E-mail address: gizem.karabulut@iuc.edu.tr (G. Karabulut).

https://doi.org/10.1016/j.surfcoat.2024.130564
Received 19 September 2023; Received in revised form 30 January 2024; Accepted 15 February 2024
Available online 27 February 2024
0257-8972/© 2024 Published by Elsevier B.V.

approach for modulating biocompatibility.

Surface modification stands out as one of the most effective methods for achieving our objectives. Various approaches have been proposed to prevent the release of metallic ions and the generation of debris resulting from wear or corrosion, among which surface modification with metal and metal oxide nanoparticles (MO NPs) agents is prominent. It is crucial to optimize the design and surface modification of metallic implants to enhance their anticorrosion properties while simultaneously ensuring biosafety and clinical effectiveness during service. Metal-based NPs exhibit improved biological, mechanical, physicochemical, and wear characteristics compared to those with grain size in the micrometer size range [10,11]. Green methods have emerged as significant contributors to the stabilizing and reducing of metal-based NPs. In comparison to chemical and physical approaches, green synthesis offers various advantages, including environmental friendliness, cost-effectiveness, and scalability for large-scale synthesis without the need for high temperature, pressure, energy, or hazardous chemicals. The substantial costs and toxicity concerns associated with traditional methods have paved the way for a low-cost, reliable, and green synthesis process [12–16]. Considerable research has focused on the applications of metal and MO NPs, such as TiO_2, Ag, Cu, CuO, Au, and Zn, primarily due to their antibacterial properties. Notably, Ag NPs and CuO NPs have shown remarkable effectiveness, displaying strong antimicrobial properties against a range of microorganisms, including bacteria, fungi, viruses, and other eukaryotic microorganisms [17,18]. Ag NPs, in particular, have found extensive use in surface treatment of orthodontic appliances [16].

In the healthcare sector, one of their applications is in the surface modification of implants, aiming to develop corrosion resistance, promote osteointegration, and, most importantly, enhance resistance against bacteria that cause infections. Studies have reported on the corrosion properties of biometals coated with metal-based NPs [6,11,13,16,19–21]. However, there is still a need for further research in this area, given the significance of the topic. Several recent studies have explored the corrosion behavior of Ag NPs coatings on stainless steel, reporting improved corrosion resistance [16,22]. Additionally, Qian et al., [23] and Jothi et al. [13] investigated the enhancement of corrosion resistance in Ag NPs-coated 316 L SS and 304SS, respectively, through electrocorrosion tests with a NaCl solution. Similarly, Tavakoli et al. [24] demonstrated improved corrosion resistance of 316 L SS through surface modification with Cu NPs-based nanocomposites. Earlier research by Roe et al. [25] introduced a cost-effective Ag NPs coating technology applicable to various substrate materials, showing promising potential in reducing infection risks. Numerous studies that were focused on enhancing of bioactivity, biocompatibility, and antibacterial properties on the surfaces of Ti through the preparation of metal/metal oxide coatings. Considering these findings, the present study aims assess the corrosion resistance of various nanocoating materials. This evaluation will guide the selection of nanocoatings for Ti6Al4V surfaces and determine the optimal application conditions. The surface modification of implant metals through the application of metal-based nanocoatings holds tremendous potential for enhancing surface properties and improving medical applications. To achieve optimal results, it is crucial to investigate the effects of several factors, including the morphological properties of the coating material, the coating method, and the drying media.

Protecting biometallic surfaces against corrosion with plant-mediated nano-based organic coatings is attractive strategy due to its efficient, cost-effective, flexible, and simplicity. While many anti-corrosion nano-coatings have been developed for this purpose, industries still seek coatings with superior need layers with better performance and lower environmental footprint. The enhancement of anti-corrosive properties of Ti-based implant materials is an area of the areas of intense interest in scientific research [6,26]. Numerous studies, both within the implant device market and the scientific literature, have aimed to enhance the utility of Ti-based implants. However, as outlined here, the question remains unresolved.

Table 1
The chemical content of Ti6Al4V.

Al, %	V, %	Fe, %	C, %	N, %	H, %	O, %	Ti, %
6.09	3.91	0.13	0.02	0.01	0.001	0.09	Balanced

In alignment with the green chemistry strategy, avoiding the use of toxic chemicals during the green synthesis of metal and metal oxide nanoparticles is a significant priority in this study. Additionally, the preferred characteristics for nanomaterials include cost-effectiveness, scalability, simplicity, and producibility under ambient conditions. Following these preferences, various bio-reducing agents derived from plant extracts were utilized in this study to produce nanostructures via the sonochemical method. These green agents not only accelerated the reduction process but also served dual roles as reducing and capping agents, effectively stabilizing the nanoparticles. Furthermore, the surface modification and effects of Ag NPs and CuO NPs on the corrosion properties of the Ti6Al4V alloy were thoroughly examined. This study specifically focuses on the corrosion properties of Ti6Al4V after surface modification with green-synthesized Ag NPs and CuO NPs derived from plant extracts. The anti-corrosion performance of the surface-modified Ti6Al4V was analyzed using different nanostructures, coating methods (drop casting and airbrush spray coating), and drying process (25 °C and 60 °C). The novelty of this research lies in optimizing corrosion resistance by comparing the application conditions of different NPs on the Ti6Al4V surface. It is anticipated that optimizing the process parameters in coating will yield efficient results and unveil new possibilities for the medical applications of Ti-based implants.

2. Materials and methods

2.1. Materials

In this study, the used substrate material was a Ti6Al4V titanium alloy bar, sourced from Varzene Metal Company (Türkiye). The chemical content of the Ti6Al4V alloy, as provided in the company's technical report, is shown in Table 1. For the synthesis of the green metal-based NPs, *Camellia sinensis* powders (matcha tea), were utilized, and these powders were obtained from Arifoğlu Company (Türkiye), were utilized. Polyethylene glycol (PEG) with a molecular weight of 400 kDa was obtained from Fluka (Switzerland). Silver nitrate ($AgNO_3$), copper (II) sulfate pentahydrate ($CuSO_4.5H_2O$), ethanol (EtOH) with a purity of $\geq$99.4 %, and sodium hydroxide (NaOH) were obtained Merck Company (Germany).

2.2. Green synthesis of Ag NPs and CuO NPs

This study employed the phyto/sonosynthesis technique to prepare Ag and CuO NPs using a biopolymeric matrix. The synthesis process involved several steps. Initially, 5 g of *Camellia sinensis* powders were added to 100 mL of distilled water and stirred at 500 rpm for 10 min. The mixture was then kept in a dark environment at room temperature for 3 days to obtain the matcha extract through decantation. In the subsequent step, 0.1 g of PEG was slowly added to the prepared extract and stirred at 500 rpm for 10 min to obtain the matrix solution. For Ag NPs, 0.1 g of $AgNO_3$ was mixed in 50 mL of distilled water for 10 min. Meanwhile, for CuO NPs, 0.0424 g of $CuSO_4.5H_2O$ was mixed in 50 mL of distilled water for 10 min. For 10 min, 0.2 g of NaOH was added to 50 mL of distilled water. In the final step, the salt solutions were mixed with the matrix solution. The process involved the dropwise addition of 4 mL of NaOH solution and 50 mL of $AgNO_3$ solution into the matrix solution, followed by mixing for 10 min to prepare Ag NPs. Similarly, 3 mL of NaOH solution and 50 mL of $CuSO_4.5H_2O$ solution were added dropwise to the matrix solution and mixed to prepare CuO NPs. Subsequently, the mixtures underwent 50 % amplitude sonication (Sonopuls HD3100,

Table 2
The identifying of the specific sample codes assignments.

Sample code	Coating material	Coating method	Temperature
AgTi-DR	Ag NPs	Drop-casting	25 °C
AgTi-DO	Ag NPs	Drop-casting	60 °C
AgTi-SR	Ag NPs	Airbrush spray	25 °C
AgTi-SO	Ag NPs	Airbrush spray	60 °C
CuOTi-DR	CuO NPs	Drop-casting	25 °C
CuOTi-DO	CuO NPs	Drop-casting	60 °C
CuOTi-SR	CuO NPs	Airbrush spray	25 °C
CuOTi-SO	CuO NPs	Airbrush spray	60 °C

Bandelin) for 30 min, and the final solutions were filtered using a sterile 0.22 μm filter at the end of the process. Detailed preparation of NPs is given in our previous articles [16,27].

2.3. Surface coating of Ti6Al4V with Ag NPs and CuO NPs

The Ti6Al4V bar, measuring of 2 mm thickness and 22 mm diameter, was prepared using a CNC turning. Subsequently, the cut pieces underwent a cleaning process in a mixture of ethanol and acetone for 10 min at 20 Hz to eliminate any impurities. After cleaning, the pieces were dried in an oven at 60 °C for 10 min. The coating process was conducted using two methods: drop-casting and airbrush spray. For the drop-casting method, 3 mL of the coating solutions were dispensed onto the entire surface of the Ti6Al4V disks using a Pasteur pipette. The solutions were dripped from four points on the substrate surface to ensure uniform coverage. A compressor kit with a 0.2 mm nozzle tip was utilized in the airbrush spray coating process. The coating solutions were sprayed onto the Ti6Al4V surfaces from a distance of 75 mm, applying a pressure of 3 bar for a duration of 4 s. To investigate the influence of different drying conditions after the coating processes, two groups were formed. The first group was allowed to dry at 25 °C for 24 h, while the second group underwent drying in an oven at 60 °C for 1 h. In total, 24 samples were prepared, with 3 samples obtained from each coating method and drying condition. To avoid any confusion, a code system was established to identify the samples, and the specific code assignments can be found in Table 2. A visual summary of the experimental procedure is provided in Fig. 1.

2.4. Characterization part

2.4.1. Characterization of synthesized Ag NPs and CuO NPs

The phyto/sonosynthesized Ag NPs and CuO NPs underwent characterization to assess their surface, chemical, and physical properties. X-ray diffraction (XRD), UV–Vis spectroscopy, and transmission electron microscopy (TEM) were employed for characterization. XRD analysis was performed using a Rigaku D/Max2200/PC device, operating at 40 kV and 15 mA with a Cu-Kα beam. Measurements were taken within the range of 20° to 80° to examine the crystal structures. UV–Vis analysis involved measuring absorbance values using a PG Instruments T80+ model dual-beam UV–Vis spectrophotometer, with the assistance of UVWin 5 software. TEM analysis was conducted using a Hitachi High Tech HT7700 device in high vacuum mode at 100 kV, allowing for the examination of the NPs at a nanoscale level. The crystallite sizes of the phyto/sonosynthesized Ag NPs and CuO NPs were determined using the Debye-Scherrer formula, as given in Eq. (2.1).

$$D_p = \frac{0.94.\lambda}{\beta.cos\,\theta} \tag{2.1}$$

The crystallite size diameter (D) was determined using the Debye-Scherrer formula, which considers the X-ray wavelength (λ) of 0.15406 nm, the Bragg's diffraction angle (θ) obtained from 2Theta (θ), and the full width at half maximum (FWHM) of the diffraction peaks.

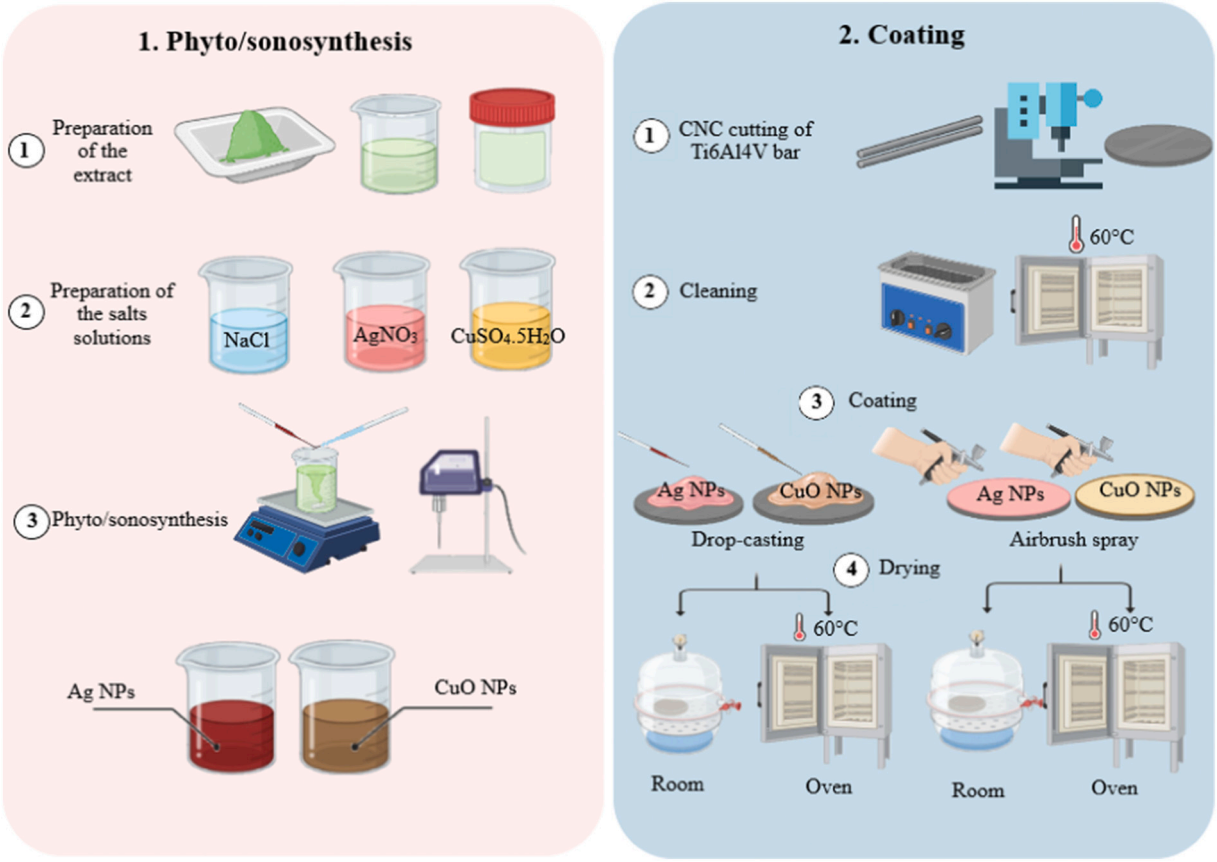


Fig. 1. Experimental steps of this study.

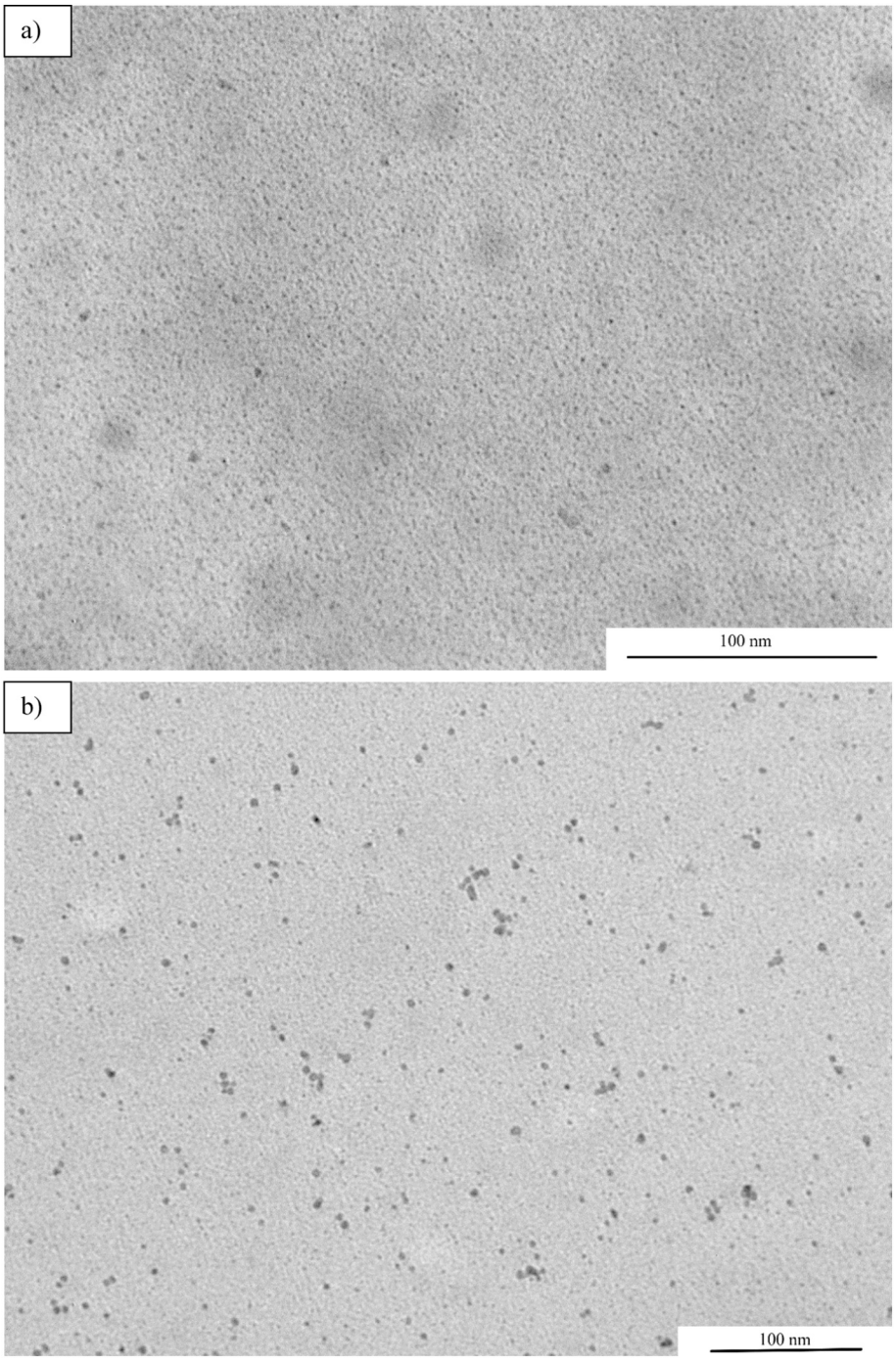


Fig. 2. TEM images of a) Ag NPs and b) CuO NPs.

2.4.2. Characterization of modified Ti6Al4V surfaces

The modified-surface with Ag NPs and CuO NPs were characterized using SEM (Zeiss-Sigma 300 device) to investigate the distribution, morphology, and size of the NPs on the Ti6Al4V disks. Additionally, the average surface roughness changes before and after NPs coating were examined using a Surftest SJ-210 model device from Mitutoyo to assess the surface texture. The ion release of the coatings was evaluated by inductively coupled plasma-mass spectrometry (ICP-MS) analysis using a ELAN9000 Perkin-Elmer device. ICP-MS analysis was used to observe the release in the coatings that gave the best results. The coated parts were placed in distilled water and kept at room temperature. Samples were taken from the solutions and examined at different intervals in 1 week.

2.4.3. Electrochemical corrosion behavior analysis

The anticorrosion performance of the surface modified Ti6Al4V alloy with different coating methods, coating materials, and drying media were evaluated using an electrochemical potentiodynamic polarization test at room temperature. For electrochemical corrosion tests, Gamry brand Interface 1000 model computer-connected potentiostat was used. All measurements were performed in Ringer's solution (pH 5.9) as the electrolyte in a 1000 mL cell to compatible with the bio-corrosive environment around an implant located inside the body. Measurements were conducted using a conventional three-electrode system, with a saturated calomel electrode as the reference electrode, a high-density graphite rod as the counter electrode, and the specimens as the working electrode. The samples were securely mounted using epoxy

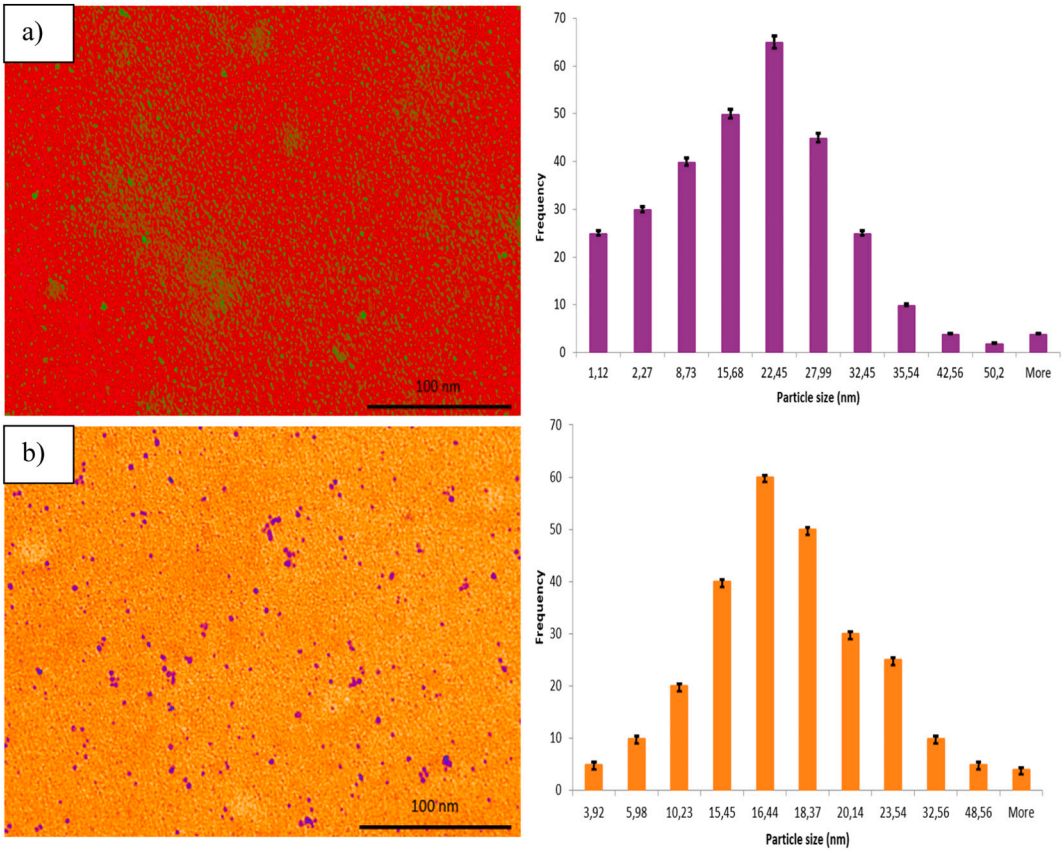


Fig. 3. AI-based TEM and average particle size distribution histograms of a) Ag NPs and b) CuO NPs.

resin and fixed to a copper cable. Initially, open circuit potential (OCP) measurements were performed until the OCP values of the specimens stabilized for 2–3 h. Once the stabilized values were achieved, Tafel tests were conducted. Tafel experiments involved scanning the potential at a speed of 1.0 mV/s within the range of −250 to +250 mV relative to the OCP values. All tests were repeated three times to ensure the reproducibility of the data in the analyzes performed using the software. The percentage of protection efficiency (%PE) provided by the NPs coating can be determined from the corrosion current density (I_{corr}) obtained from the Tafel curves using the formula as given in Eq. (2.2) [28].

$$(PE\%) = \frac{i_{corr(bare)} - i_{corr(coated\ sample)}}{i_{corr(bare)}} \times 100 \quad (2.2)$$

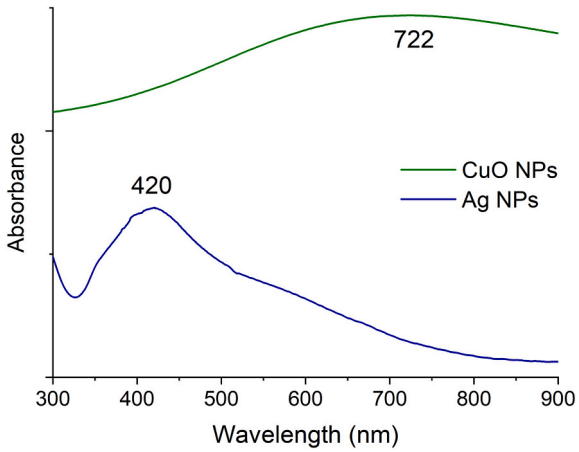


Fig. 4. UV–Vis results of the phyto/sonosynhtesized NPs.

3. Results and discussion

3.1. Characterization results of the phyto/sonosynthesized Ag NPs and CuO NPs

The phyto/sonosynthesized Ag NPs and CuO NPs were characterized using TEM analysis to determine the particle size and distribution in the solution. In Figs. 2 and 3, TEM images, along with AI-based analysis and particle size distribution histograms, were presented. The AI-supported analysis utilized advanced algorithms to accurately identify and analyze individual NPs within the TEM images. This approach allowed for a more precise assessment of the particle size distribution and provided valuable insights into the nanoscale morphology of the Ag NPs and CuO NPs. A simple image analysis technique using ImageJ software was utilized to effectively analyze densely clustered and small NPs in TEM images. This approach enabled accurate characterization of the size, shape, and distribution of NPs, providing valuable insights into the nanomaterials studied. In this study, we utilized an ImageJ-based TEM analysis technique to assess and analyze green Ag NPs and CuO NPs. The characterization of Ag NPs and CuO NPs were performed using specific RGB and ICA modes, employing color-corrected images in 8-bit format. To improve the differentiation between the outlined NPs and the background matrix, the images were analyzed using the red-blue-green (RGB) technique. This approach enhanced the separation and quantification of the NPs, leading to more precise analysis. The particle sizes of the synthesized Ag NPs (green color) and CuO NPs (green color) were determined using AI-supported TEM images analyzed with ImageJ software. The particle sizes of the synthesized Ag NPs and CuO NPs were determined using AI-supported TEM images analyzed with ImageJ software. The TEM images of the Ag NPs were captured in RGB mode, with a resolution of 962 × 608 pixels and the green color channel was used for analysis. On the other hand, the TEM images of the CuO NPs

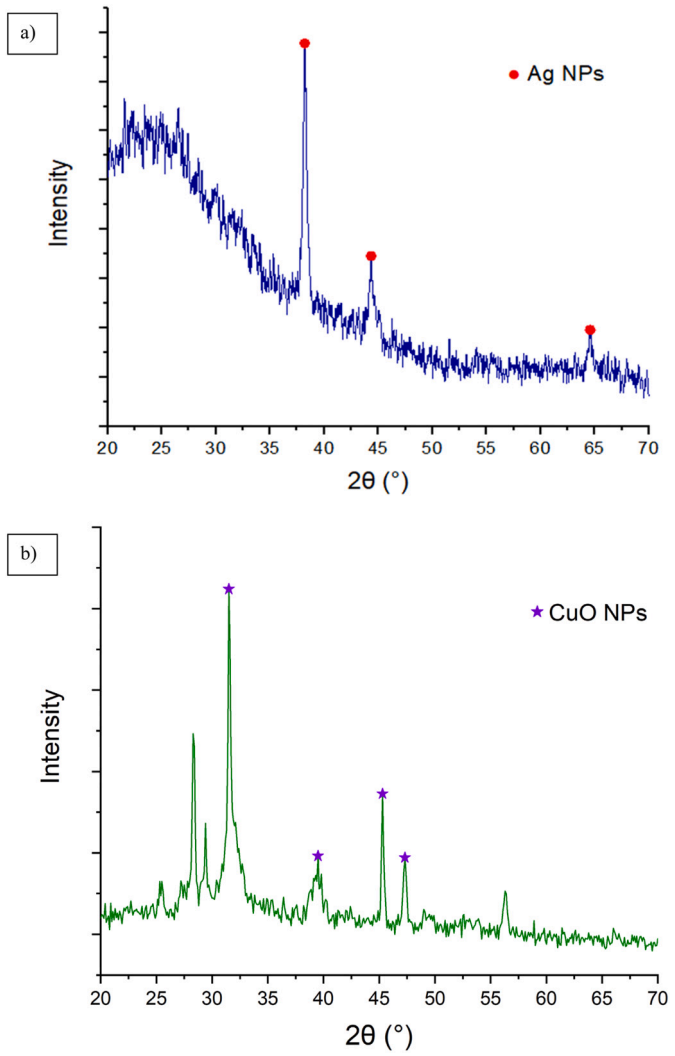


Fig. 5. XRD spectra of the phyto/sonosynhtesized a) Ag NPs and b) CuO NPs.

were captured in ICA mode, with a resolution of 954 × 642 pixels and the purple color channel was used for analysis. As a result of the study, the average particle size of the Ag NPs was approximately 16.44 nm, while the CuO NPs had an average particle size of around 22.45 nm.

The UV–Vis method is a typical technique for determining of the type of NPs and their dispersion properties in the solution [29]. Metal-based NPs, due to their high specific surface area (SSA) properties, exhibit surface plasmon resonance (SPR) and produce observable radiation in UV–Vis analysis, allowing for the determination of their properties [30]. Fig. 4 presents the UV–Vis spectra of the synthesized Ag NPs and CuO NPs. In this study, the phyto/sonosynthesized Ag NPs using matcha tea extract demonstrated a relatively narrow peak at 420 nm, while CuO NPs exhibited a broad peak at 722 nm. In literature, characteristic spectra of Ag NPs have been observed between 400 and 500 nm in the phytosynthesis technique [31–33]. It is worth noting that the literature contains significantly different values in studies on the phytosynthesis of CuO NPs, which can be attributed to variations in the appearance of oxide bands in the spectrum due to different structures [34]. The broadness of the peaks in the UV–Vis spectrum indicates a polydisperse distribution. The broader spectrum observed for CuO NPs suggests a higher degree of polydisperse distribution compared to Ag NPs, which is consistent with the TEM images obtained.

The XRD graphs of Ag NPs and CuO NPs are given in Fig. 5. In Fig. 5 (a), characteristic peaks are observed at 2θ = 38.2°, 44.3°, and 64.5°, corresponding to the (111), (200), and (220) planes of Ag, respectively. This indicates that the Ag nanostructure possesses a face-centered cubic (FCC) structure [32,35]. The peak observed at 21.3° is attributed to the presence of the organic phase [36]. In Fig. 7(b), the peaks observed at 2θ = 31.5°, 39.5°, 45.4°, 47.3°, 56.3°, and 75.1° correspond to the (110), (111), (−112), (−202), (021), and (222) planes of CuO, respectively. This indicates that the CuO nanostructure exhibits a monoclinic structure [37]. Additional peaks at 25.5°, 28.3°, and 29.4° can be attributed to organic phases. The diffraction patterns of Ag NPs and CuO NPs are consistent with the JCPDS files 00-004-0783 and 04-015-5865, respectively. The crystalline sizes of the NPs were calculated using the Debye-Scherrer formula, as given in Eq. (2.1), resulting in sizes of 27 nm for Ag NPs and 33 nm for CuO NPs.

Water-soluble phenolic compounds identified in *Camellia sinensis*, such as epicatechin (EC), catechin (C), epigallocatechin (EGC), and epigallocatechin gallate (EGCG), play a significant role in the bio-mediated synthesis of Ag NPs. Acknowledged as the primary phenols in green tea, polyphenolic compounds, particularly catechins, are highlighted in existing literature for their pivotal function in strongly reducing Ag^{+} ions, potentially leading to the formation of Ag NPs [38]. The reduction of silver ions commences as these polyphenols contributes electrons. Additionally, these compounds act as effective capping agents, preventing aggregation and ensuring the stabilization of the generated Ag NPs. The reduction process is further facilitated by polyphenol-silver ion exchange and chelation processes. In addition, CuO NPs were formed when polyphenols in the extract attached to Cu^{2+} ions, generated upon dissolving $CuSO_4$ in water. Subsequently, these metal complexes underwent reduction, resulting in the formation of CuO particles. The processes of aggregation and nucleation are integral stages in the particle formation. Previous research has demonstrated analogous methods for NPs production [37]. This study underscores the bio-mediated synthesis of Ag and CuO NPs in *Camellia sinensis*, revealing the intricate interactions among polyphenolic chemicals, reduction processes, and stabilizing mechanisms. This approach offers a promising avenue for the environmentally friendly production of nanoparticles.

3.2. Characterization results of the modified Ti6Al4V surfaces

While there are numerous studies in the literature about the surface modification of metal substrates with Ag NPs [13,16,22,39–42], there are very few studies on the surface modification of metal substrates with CuO NPs [24]. In this study, the surfaces of Ti6Al4V alloy parts, which are frequently preferred in biomedical applications, were modified using the drop-casting and airbrush spray coating methods. The morphology of the NPs on the surfaces and the effect of the coating on the corrosion resistance of the substrates were investigated, considering the different drying mediums. In Fig. 6, SEM-EDX images illustrate the use of different drying mediums for Ti6Al4V parts that have underwent surface modification with Ag NPs using two distinct methods. Fig. 6a displays samples prepared through the drop-casting method and dried at 25 °C. The images reveal complete surface coverage by spherical Ag NPs, displaying a wide size distribution ranging from 30 nm to 200 nm, along with notable particle agglomerations. Conversely, Fig. 6b depicts samples modified using the same method but subjected to drying at 60 °C. Here, it can be observed that Ag NPs tend to adopt a closer-to-spherical shape and distribute within a narrower size range, but with significant overlapping. This phenomenon can be attributed to the rapid evaporation of water from the surface and the proximity of particles during oven drying. Moving on to Fig. 6c and d, these images depict the surfaces modified using the airbrush spray coating method and dried under room conditions and oven conditions, respectively. In Fig. 6c, it is evident that the samples dried at room conditions exhibit more pronounced agglomeration, with large NPs displaying significant deviation from spherical shape. While the NPs exhibit an independent distribution, a homogeneous size distribution is not observed. On the other hand, Fig. 6d displays the images of samples prepared using the airbrush spray coating method and dried in an oven. In these samples, the NPs maintain

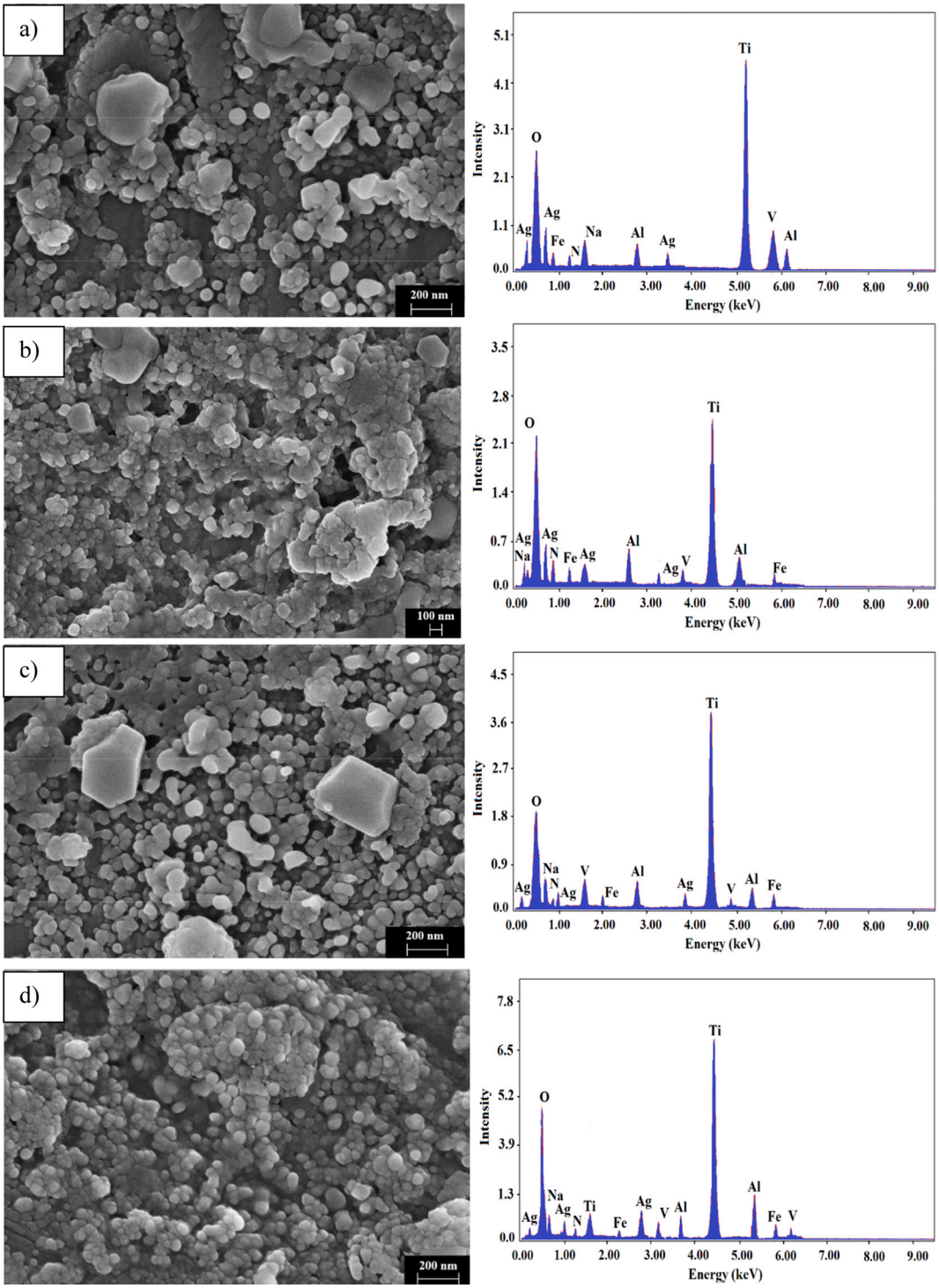


Fig. 6. SEM-EDX images of Ag NPs coated samples: a) AgTi-DR, b) AgTi-DO, c) AgTi-SR, and d) AgTi-SO.

their small size and exhibit a narrow size range. The distribution on the surface appears to be more homogeneous. When comparing the two methods, it is evident that the airbrush spray coating method leads to surface modification with smaller-sized NPs. Additionally, the choice of the drying medium significantly influences the size and agglomeration state of the Ag NPs. As is known, smaller-sized and independent NPs further enhance the strength properties of the surfaces. In the EDX results, presence of Ag is due to the presence of Ag NPs, while the presence of Na atoms is due to the plant extract. The presence of the O atom is due to the oxidation of Ag ions. Ti, Al, V, and trace amounts of Fe atoms observed in the coated surface are from the elemental signatures of the Ti6Al4V alloy substrate material.

Fig. 7a–d presents SEM-EDX images of the surfaces modified with CuO NPs. In all samples, the CuO NPs exhibit a spherical shape. On the coated surfaces prepared using the drop-casting method, noticeable cracks are observed in the sample dried at 25 °C. The dried sample in the oven medium exhibits CuO NPs distributed in two distinct sizes: small (~30 nm) and large (~100 nm). Notably, there are pores present in the coating at certain points (Fig. 7b). Conversely, the CuO NPs coatings performed by the airbrush spray coating method display a more

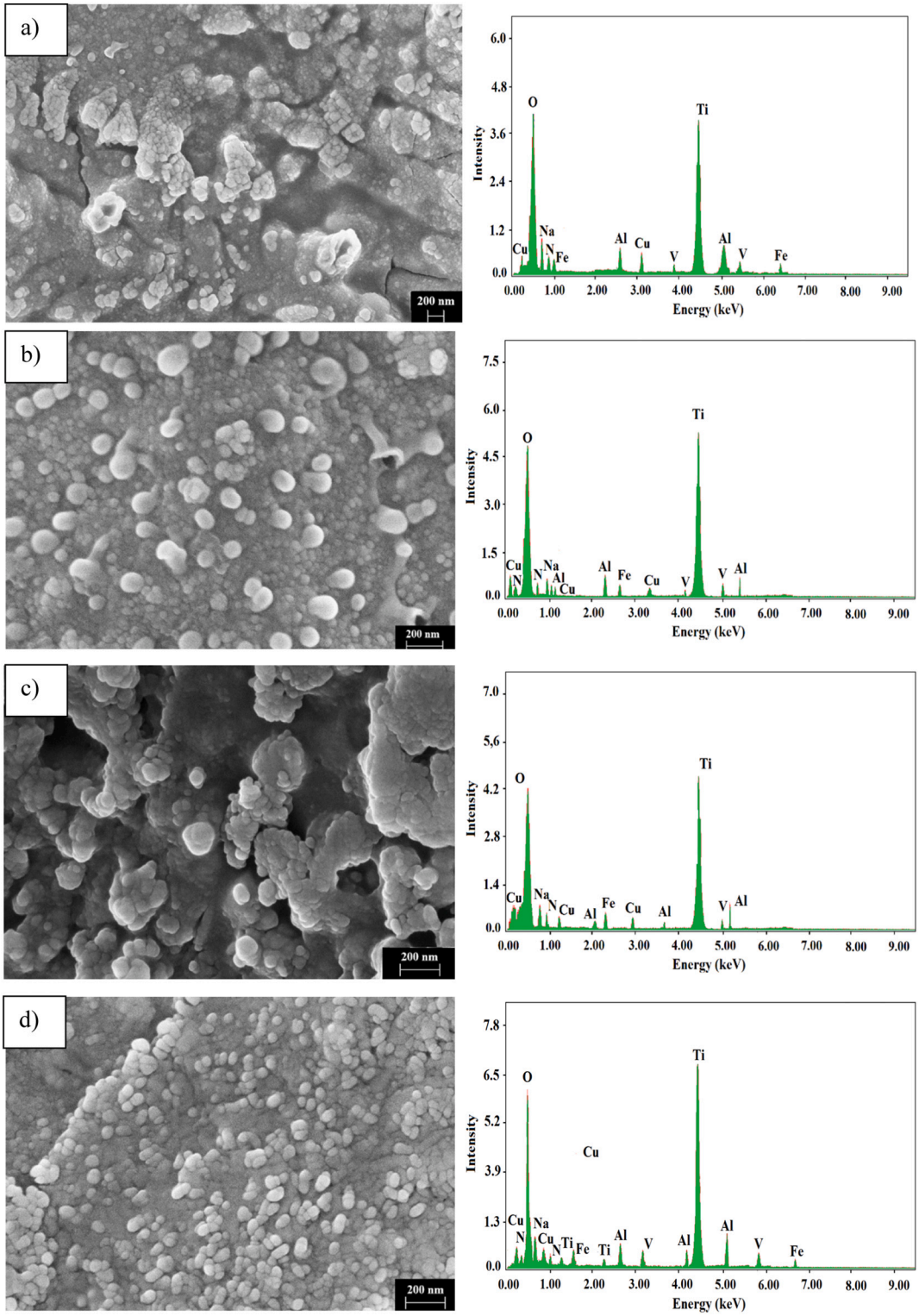


Fig. 7. SEM-EDX images of CuO NPs coated samples a) CuOTi-DR, b) CuOTi-DO, c) CuOTi-SR, and d) CuOTi-SO.

homogeneous size distribution. Additionally, the SEM image (Fig. 7c) of the sample coated with the airbrush spray technique and dried at 25 °C reveals a relatively layered appearance. It is evident that CuO NPs exhibit superior characteristics in terms of size distribution and homogeneous distribution on the surface. Regarding size distribution and the homogeneity of CuO NPs coating on the surface, it is observed that the surface dried under oven conditions and coated with the airbrush spray technique exhibits the best results. When comparing the behavior of different NPs, Ag NPs display greater morphological variability, while there are no significant differences between methods for CuO NPs. Notably, CuO NPs demonstrate a more homogeneous behavior in terms of size distribution and shape compared to Ag NPs. Overall, it was observed that employing the airbrush spray coating method and drying with an oven resulted in smaller-sized NPs, reduced agglomeration, and a more homogeneous surface modification. The explanations in EDX measurements of Ag NPs are also valid for EDX measurements of CuO

Table 3
The average surface roughness values of the bare and NPs coated surfaces.

Specimen code	Uncoated value (Ra, μm)	Coated value (Ra, μm)
AgTi-DR	1.784 ± 0.075	1.621 ± 0.117
AgTi-DO	1.871 ± 0.067	1.586 ± 0.096
AgTi-SR	1.612 ± 0.088	1.486 ± 0.077
AgTi-SO	1.763 ± 0.126	1.479 ± 0.103
CuOTi-DR	1.896 ± 0.093	1.672 ± 0.109
CuOTi-DO	1.798 ± 0.121	1.587 ± 0.106
CuOTi-SR	1.921 ± 0.137	1.586 ± 0.095
CuOTi-SO	1.898 ± 0.102	1.578 ± 0.059

NPs.

A lot of implant features affect the osseointegration of implant materials which is conducive to bone bonding. These features include implant geometry, design, and connection, and surfaces characteristics of the implant. Among them, the surface roughness of implants is an essential determinant of long-term and short-term clinical performance [43,44]. In this study, the average surface roughness values before and after coating, prepared with different coating methods and drying mediums, are given in Table 3. According to the average surface roughness measurement results, it has been observed that the values of the coated surfaces in all coating conditions were lower than the uncoated Ti6Al4V alloy. The surface roughness values of AgTi-DR, AgTi-DO, AgTi-SR and AgTi-SO coded samples decreased by 8.9 %, 15.2 %, 12.7 and 16.1 %, respectively, after coating. Similarly, the values for CuOTi-DR, CuOTi-DO, CuOTi-SR and CuOTi-SO coded samples decreased by 11.8 %, 11.7 %, 12.9 and 16.8 %, respectively. This reduction is attributed to the coating of linear spaces formed on the surface of the Ti6Al4V alloy because of machining with nanoscale particles. Closing the micro and nano-scale gaps on the material surface is crucial for achieving better corrosion resistance [45]. In both coatings, the influence of the coating method and drying medium on the surface roughness values nearly identical. A rough surface is a crucial characteristic for metallic surfaces intended for biomedical applications. The adhesion, spread, and growth of cells on the implant material are contingent on surface roughness, while increasing surface roughness inhibits chemical stability, microhardness, and bacterial adhesion [16,46]. Surface roughness values for certain metallic-based biomaterials are categorized as fine between 0.5 and 1 μm and medium between 1 and 2 μm [47]. The samples with a medium surface roughness value before coating remained within this range after coating. This outcome suggests the potential use of the coated parts in biomedical applications. Jiang et al. reported that the Ra values after coating were similar to those before coating, ensuring surface smoothness, which is crucial for chemical stability [2]. Additionally, Theimer et al. noted in their study that the surface roughness of the coating is linked to whether the particulate structure is coarse or fine, exerting significant effects on corrosion resistance [48]. Another study by Zhang et al. found that the average surface roughness value of the coated surface affects various properties such as surface activity characteristic, abrasive, and interaction with bacteria [44].

Figs. 8 and 9 show 3D profilometer images of materials' surfaces modified with Ag NPs and CuO NPs, respectively. In the images, black regions represent the deepest areas, while white regions represent the upper areas. There are obvious deep areas in the images of all samples due to the CNC cutting process. In the images, it is generally evident that the samples prepared by the airbrush spray coating method have a thinner coating thickness and a rougher structure.

3.3. Electrochemical corrosion test results

Corrosion is a pervasive challenge encountered in various fields, particularly in biomedical applications. Its detrimental effects include material deterioration and potential harm to human health, such as ion release, inflammation, and toxicity [13,41]. Therefore, studying the corrosion behavior of materials is crucial to ensure the safety and effectiveness of biomedical devices. Materials chosen for biomedical applications are selected based on their high specific strength and excellent corrosion resistance, making them suitable for long-term implantation within the human body [49]. However, their corrosion resistance can be compromised by factors such as the presence of physiological fluids and mechanical wear caused by body movement. Despite Ti6Al4V being a biometal with strong corrosion resistance, it can still corrode under certain environmental conditions, especially when the protective passive layer on its surface is damaged [24]. To address these challenges, surface modification techniques utilizing Ag NPs and CuO NPs have been explored as potential solutions in this study. The objective is to develop the corrosion resistance of Ti6Al4V alloy through these surface modifications, thereby improving the longevity and reliability of biomedical devices.

Figs. 10 and 11 present the electrochemical corrosion investigations for both bare substrate and coated surfaces. In Fig. 10a and b, the Open Circuit Potential (OCP) measurements are displayed for surfaces coated with phyto/sonosynthesized Ag NPs and CuO NPs, respectively. OCP curves offer insights into the sample's inertness in the solution medium, with a more stable OCP indicating higher inertness [50]. As shown in Figs., all the OCP values of the Ti6Al4V alloys coated with NPs shifted positively after coating. OCP shift in the noble direction refers to the formation of a passive film that acts as a barrier to metal dissolution and reduces the rate of corrosion. Some studies have reported that passivation layer formation occurs with a rapid increase in OCP in the initial 1000 s [41]. In comparison, the OCPs of the airbrush spray-coated and dried in the oven samples remained the highly stable at a relatively consistent level throughout the entire test period. Notably, the CuO NPs coatings (−0.206 V for CuOTi-SO and −0.132 V for CuOTi-SR) presented more negative OCPs compared with the Ag NPs coating (−0.132 V for AgTi-SO and −0.102 V for AgTi-SR) and the corrosion potentials tend to decrease with time. The airbrush spray-coated samples had the highest OCP values. The increase in OCP may be attributed due to the more homogeneous distribution of coatings on the surface, both in terms of size and coating. Additionally, the improved corrosion resistance observed under oven drying conditions suggests a denser coating on the surface. These results align with the SEM findings, which indicate a smaller particle size and a denser morphology on the AgTi-SO and CuOTi-SO coated surfaces compared to those of AgTi-DO and CuOTi-DO coatings. This microstructural condition reduces the specific surface area (SSA) and enhances corrosion resistance [12]. The airbrush spray coating method enables the production of dense coatings with small pores, yielding smoother and more easily dried results [42]. Changes in surface morphology, such as a reduction in crystalline size, increased porosity, surface roughness, and compactness, as reported by Bir et al., inhibit the ion diffusion process and further enhance the substrate's corrosion protection [51]. Echavarria et al. stated that the highest corrosion density and electrochemical activity level was in Ag NPs due to the high specific contact area resulting from their small size. Previous studies in the literature have highlighted that the presence of smaller and spherical grains in NPs-based coatings is an effective approach to prevent the transport of corrosion products and the long-term propagation of microcracks [13,52].

Fig. 11a and b shows the polarization curves of the uncoated and Ag NPs and CuO NPs coated samples, respectively. Corrosion current densities (I_{corr}) and corrosion potentials (E_{corr}) were directly derived from the polarization curves using Tafel extrapolation. Smaller I_{corr} and larger E_{corr} values typically indicate to better corrosion resistance. E_{corr} serves as a corrosivity test to determine how well a substrate is protected after coating. The rise in the E_{corr} value corresponds to an increase in the protection efficiency (PE) [53]. As shown in the Fig. 11, all the coatings exhibited markedly lower I_{corr} and more positive E_{corr} than the uncoated substrate. The low I_{corr} values of the coatings indicate that NPs coatings act as a barrier between the Ti6Al4V substrate and the electrolyte solution and they are inversely proportional to the corrosion rate. The values of OCP, E_{corr}, I_{corr} and PE% are summarized in Table 4, along with

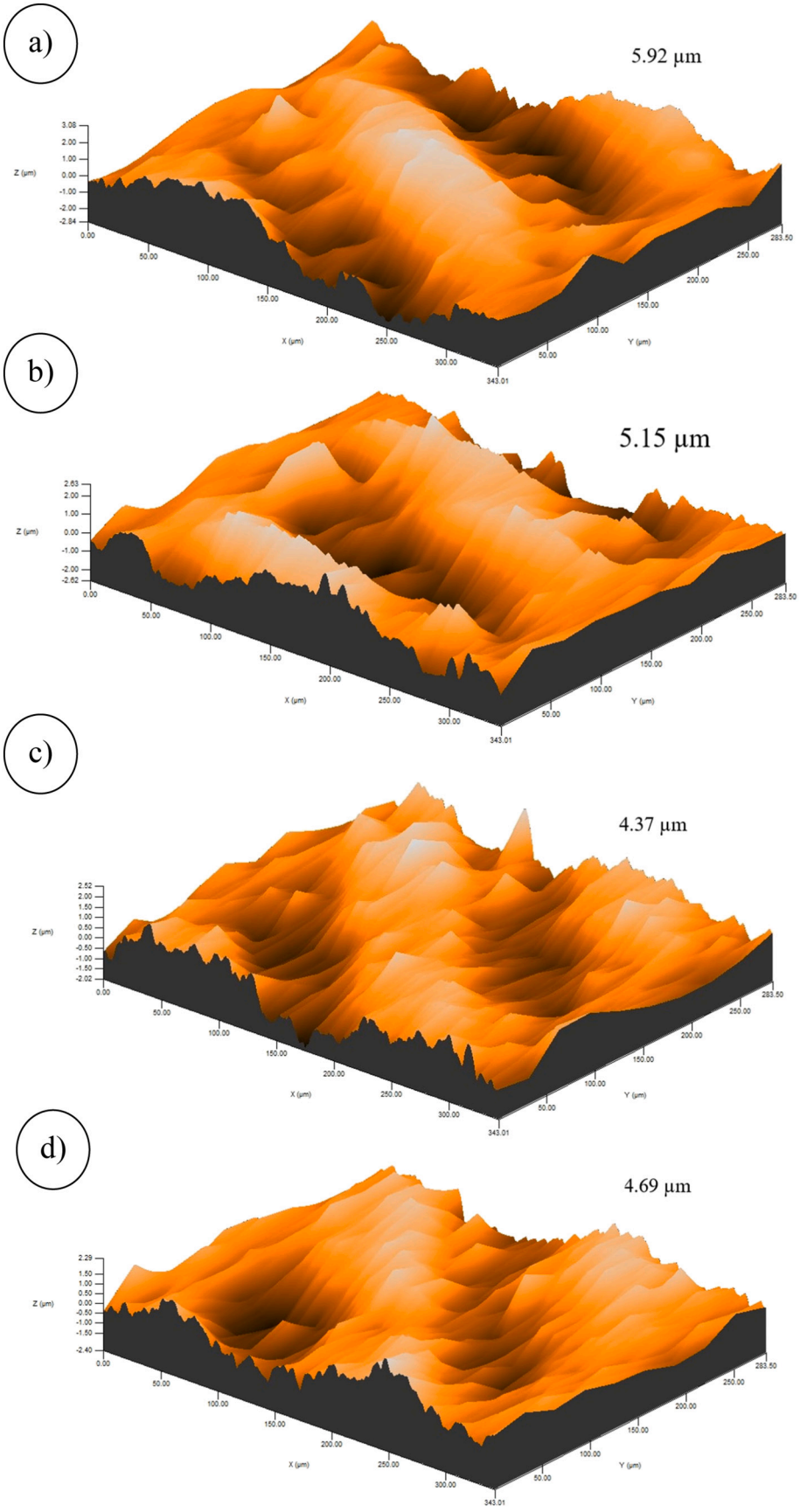


Fig. 8. 3D profilometer results of Ag NPs coated Ti6Al4V surfaces a) AgTiDR, b) AgTiDO, c) AgTiSR, and d) AgTiSO.

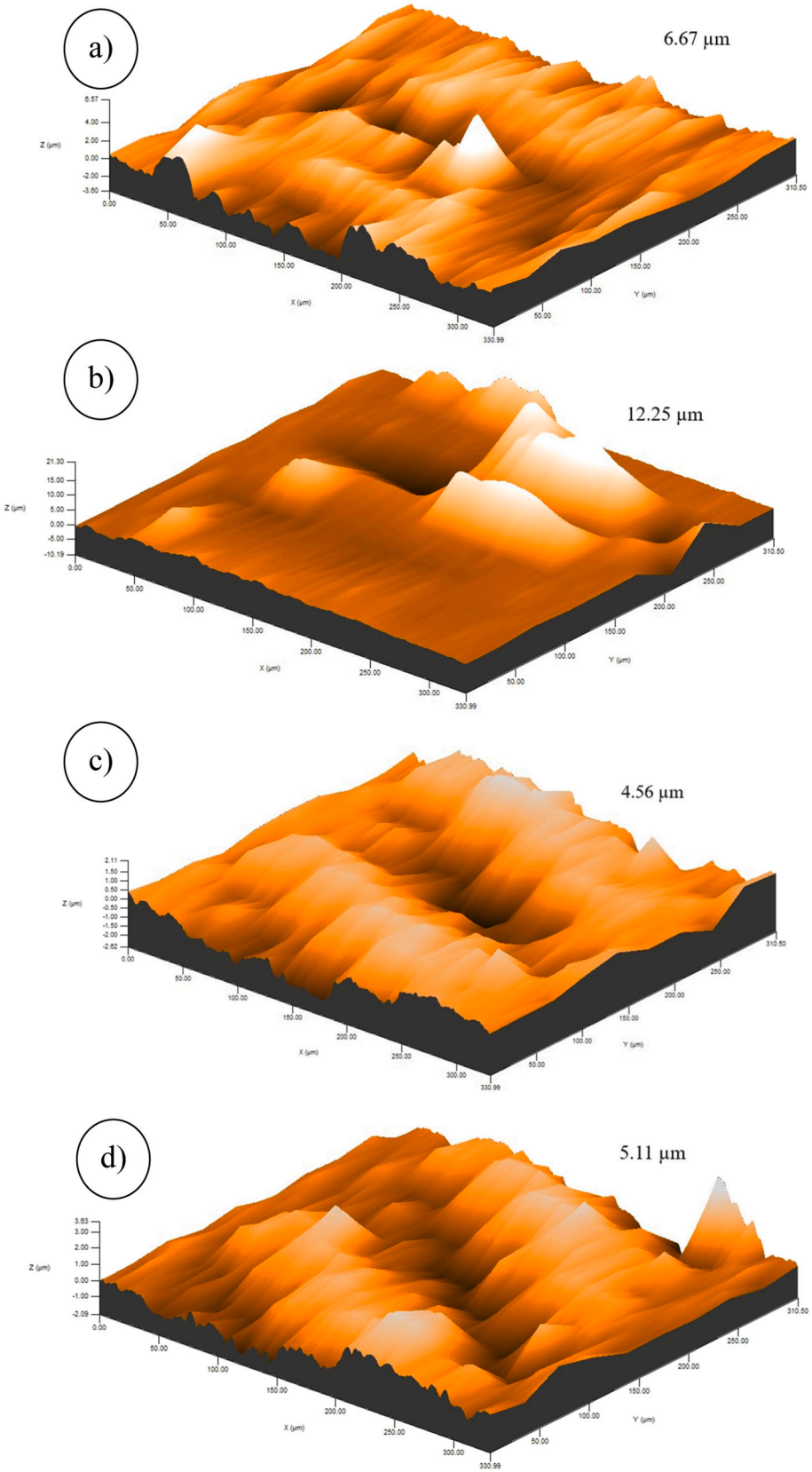


Fig. 9. 3D profilometer results of CuO NPs coated Ti6Al4V surfaces a) CuOTiDR, b) CuOTiDO, c) CuOTiSR, and d) CuOTiSO.

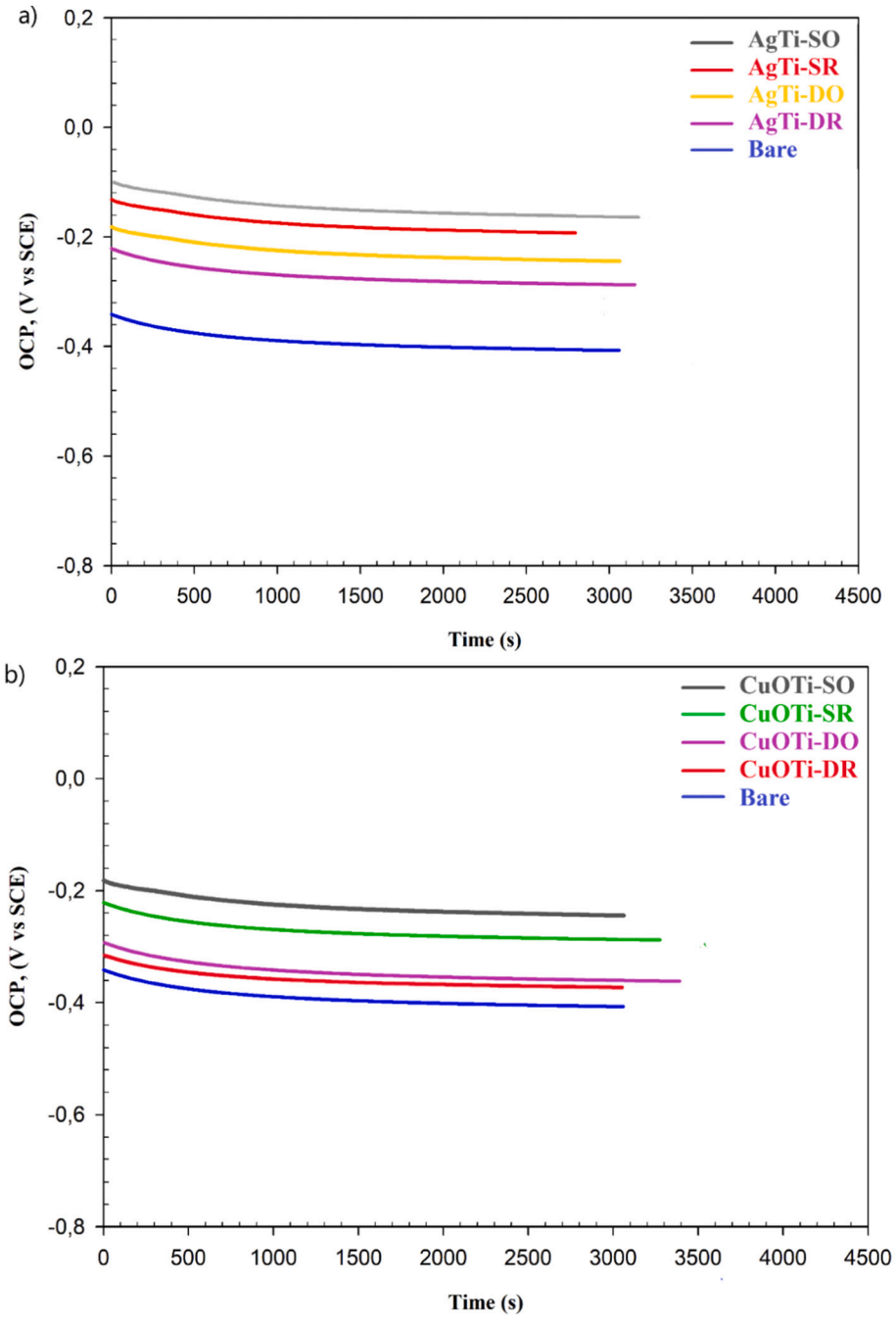


Fig. 10. OCP curves of the bare and coated samples a) Ag NPs and b) CuO NPs.

the protection efficiency of the coatings based on these values. The I_{corr} values of the AgTi-SO and CuOTi-SO coded coatings were one order of magnitude lower than those of the AgTi-DO and CuOTi-DO coded samples, demonstrating superior corrosion protection. Particularly in the airbrush spray coating, the I_{corr} values of the Ag NPs coated substrates (0.450 μA/cm^2 for AgTi-SO and 0.213 μA/cm^2 for AgTi-SR) were approximately one magnitude lower than the CuO NPs coated subtracts substrate (0.924 μA/cm^2 for CuOTi-SO and 0.766 μA/cm^2 for CuOTi-SR), indicating an enhanced corrosion protection. The Ag NPs with spherical small-sized granular structure uniformly distributed over the surface to improve the corrosion resistance. I_{corr} is a crucial parameter for determining corrosion behavior [41], suggesting that CuO NPs coating may exhibit lower corrosion resistance compared to Ag NPs coating. Considering the results of polarization and surface roughness are considered together; it can be concluded that a smoother surface after coating (lower Ra values) provides better corrosion protection. This is supported by the low probability of micron and submicron cracks on smooth surfaces, as reported in the literature. Grayeli-Korpi and Savaloni highlighted that smoother surfaces showed higher resistance in corroding medium, and an increase in implantation energy improved corrosion resistance [19]. For this reason, it is of great importance to adjust the porous structure resulting from the surface properties of the coating. Normally, the porous coating structure can be tuned by easily optimizing oxidation parameters such as voltage, current density, and frequency [54].

Fig. 12 presents the PE% of the coatings. Overall, all results indicate that NPs coating can effectively enhance the anticorrosive performance of the Ti6Al4V alloy substrate. The outcomes that the NPs effectively

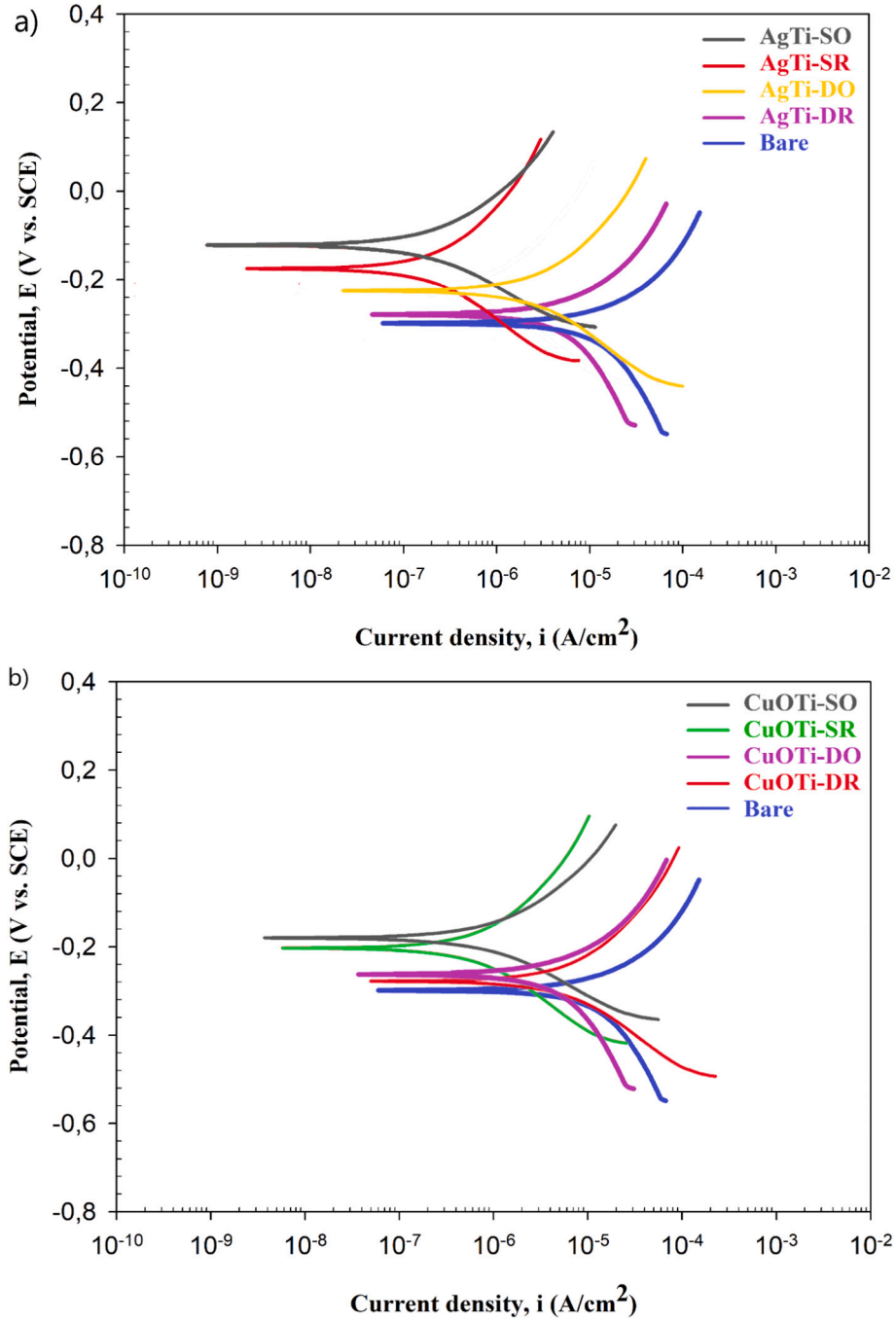


Fig. 11. Tafel curves of the bare and coated samples a) Ag NPs and b) CuO NPs.

Table 4
Electrochemical corrosion test results of the samples in Ringer's solution.

Sample code	OCP (V)	E_{corr} (mV)	I_{corr} (μA/cm^2)	Protection efficiency PE (%)
Bare	−0.343	−308	8.115	–
AgTi-DR	−0.223	−277	7.049	13.14
AgTi-DO	−0.181	−222	5.553	31.57
AgTi-SR	−0.132	−172	0.450	94.45
AgTi-SO	−0.102	−124	0.213	97.37
CuOTi-DR	−0.287	−272	7.71	4.99
CuOTi-DO	−0.266	−260	7.12	12.26
CuOTi-SR	−0.206	−202	0.924	88.61
CuOTi-SO	−0.132	−176	0.766	90.56

covered the surface of the Ti6Al4V alloy, forming a protective layer. This layer acted as a barrier, preventing corrosive agents, particularly Cl^- ions, from contacting the surface. In the literature, investigations into the corrosion resistance properties of metallic surfaces modified with NPs utilized various corrosion measurement techniques in different environments, such as NaCl [13], Ringer's solution [16,22], and phosphate buffer solution (PBS) [41]. These studies have demonstrated that the corrosion resistance can vary under different conditions and over time, with a notable decrease in corrosion resistance observed, particularly in the presence of NaCl [13]. In this study, the corrosion resistance measurements conducted in Ringer's solution yielded consistent results with similar studies in the literature [16,22]. This reinforces the reliability and relevance of the obtained corrosion resistance data in the chosen experimental environment.

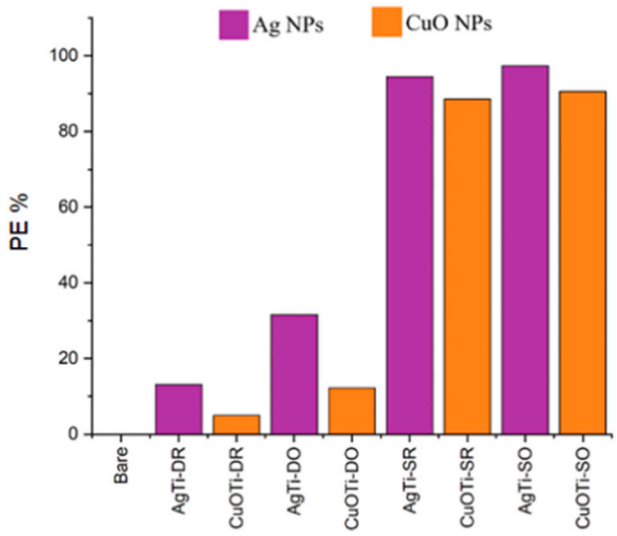


Fig. 12. Protection efficiency (PE) of bare and coated samples.

Table 5 summarizes the corrosion behavior of Ti-based materials whose surfaces have been modified with various nanomaterials using different methods. There are many studies in the literature to improve the corrosion resistance of metallic substrates [27,41,42,51,55,56]. Recent developments in nanotechnology have significantly enhanced corrosion-resistant coatings by enabling the creation of advanced nanostructured materials that offer superior protection against corrosion, extending the lifespan of various metallic surfaces and infrastructure. As seen in the table, NPs are useful in improving the corrosion behavior of Ti-based substrates. The green Ag and CuO NPs synthesized in this study highlight an important result by improving the corrosion behavior of the substrate material very well.

After implantation, metal-based implants are subjected to various corrosion reactions within the body environment. Therefore, it is crucial to enhance the stability and thickness of passive oxide layers in various ways to prevent the release of metallic ions and particles that would reduce the corrosive effects [12]. The effectiveness of the Ag NPs and CuO NPs coatings to prevent corrosion on the Ti6Al4V substrate is referred to as corrosion resistance. Corrosion resistance involves the development of a protective barrier on the substrate surface, the release of ions with antibacterial characteristics, and the prevention of corrosive processes. These coatings work to reduce or stop the substrate material's deterioration when exposed to corrosive conditions. In the case of Ag NPs coating on the Ti6Al4V substrate, the oxidation of Ag to Ag ions (Ag^+) can occur during corrosion reactions. The representation of this process is as follows:

$$Ag \rightarrow Ag^+ + e^- \quad (2.3)$$

The release of Ag^+ ions into the environment can influence corrosion behavior and provide a certain level of protection to the Ti6Al4V substrate. Similarly, in the case of CuO NPs coating, the oxidation of Cu to Cu ions (Cu^{2+}) and the reduction of an oxidizing agent, such as oxygen (O_2), can occur during corrosion processes. The reactions can be represented as follows:

$$Cu \rightarrow Cu^{2+} + 2e^- \quad (2.4)$$

$$O_2 + 2H_2O + 4e^- \rightarrow 4OH^- \quad (2.5)$$

$$\text{Overall reaction}: 4Cu + O_2 + 2H_2O \rightarrow 4Cu^{2+} + 4OH^- \quad (2.6)$$

The corrosion mechanisms of Ag NPs and CuO NPs coatings can involve several processes, including:

- Passivation: The coating with Ag and CuO NPs promotes the growth of a passive oxide layer on the surface. This oxide layer acts as a barrier against corrosive species, significantly slowing down the corrosion rate.
- Galvanic Protection: The NPs (Ag or CuO) in the coating undergo sacrificial corrosion in the presence of an electrolyte, providing protection to the underlying substrate material.
- Regulation of pH: The coatings can regulate the pH of the surrounding environment, helping minimize the corrosive effects of acidic or alkaline solutions.
- Self-Healing: The coatings release ions (Ag^+ or Cu^{2+}) that can interact with bacteria or corrosive species, inhibiting corrosion processes and promoting self-healing of the coating.

The corrosion characteristics of nanostructured metal-based coatings are directly dependent on the morphology and surface properties, as well as the chemical properties of the NPs. The design of metal-based nanostructures and the modification of surfaces need to be optimized to increase biological safety and clinical efficacy during use, all while maintaining the good corrosion and mechanical properties of the base substrate materials.

3.4. Silver and copper release tests

ICP-MS analysis was used to observe the ion release in Ag and CuO NP coatings, which gave the best results. The amount of silver and copper ions released from the coated surfaces was measured. Fig. 13 shows the table showing the measurement results performed at regular intervals. The graphs show that the amount of ions passing into the solution increased throughout the day. As expected the amount of ions released increased with time. Ag and CuO NPs are multifunctional and protect the Ti6Al4V surface while also reacting over time for intrabody reactions. As stated in the literature, reactions occur between 12 h and 10 days after implantation in early stage [57]. In this case, the release behavior shown can be interpreted as sufficient. The results are

Table 5
Comparison of Ti-based surfaces coated with various NPs.

Testing materials	Coating method	Test method	Result	References
Ti6Al4V coated with CuO NPs prepared from *Murraya koenigii* leaf	Electrodeposition	Potentiodynamic polarization	%58.15 protective	Devadoss et al., 2023 [55]
TiAlZr coated with Ag NPs	Dip coating	Dynamic polarization test	Better corrosion behavior	Ionita et al., 2011 [57]
Ti6Al4V coated with TiO_2 NPs	Spin coating	Potentiodynamic polarization	Better corrosion behavior	Höhn and Virtanen, 2015 [58]
Ti6Al4V coated with TiO_2 NPs	Spin coating	Potentiodynamic polarization	More corrosion resistant	Zaveri et al., 2009 [59]
Porous Ti6Al4V (%50) coated with Chitosan/Ag NPs	Electrodeposition	Anodic polarization	%96 protective	Cabezon et al., 2021 [60]
Ti6Al4V coated with Ag NPs	Airbrush Spray Coating	Potentiodynamic polarization	%97.37 protective	In this study
Ti6Al4V coated with CuO NPs	Airbrush Spray Coating	Potentiodynamic polarization	%90.56 protective	In this study

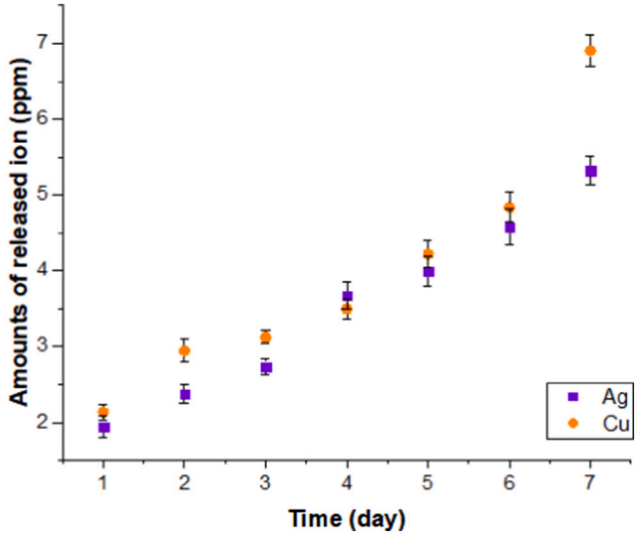


Fig. 13. Ag and Cu ions release results from surface-modified samples.

consistent with the literature [57,61–63]. The graph shows that Cu from the samples coated with CuO NPs is released faster than the release of Ag from the samples coated with Ag NPs. This can be interpreted as overlapping with other results.

4. Conclusions

The objective of this study was to assess the corrosion resistance of Ti6Al4V alloy surfaces coated with multifunctional Ag NPs and CuO NPs synthesized through a green sonochemical method in an organic biomatrix. Varying the coating method and drying temperatures aimed to identify optimal conditions for corrosion resistance, crucial for biocompatibility. The key findings, emphasizing the study's unique contributions, are succinctly summarized:

- Successful synthesis of Ag NPs and CuO NPs using a green sonochemical method, showcasing its applicability, cost-effectiveness, and eco-friendliness.
- Homogeneous distribution of spherical-shaped Ag NPs and CuO NPs in the biopolymeric matrix, with average sizes of approximately 16.44 nm and 22.45 nm, respectively.
- The dispersion of NPs was more homogeneous, and agglomeration was less, especially for surfaces that were room-dried and subsequently oven-dried.
- Ra values of all the superficially modified Ti6Al4V alloys slightly decreased and within a medium classification, compatible for use in implant materials. The protectiveness of the coating improved with decreasing Ra values.
- The results demonstrated the importance of surface modification in achieving appropriate corrosion resistance, as all the surface-modified samples showed a more positive E_{corr} and a lower I_{corr}.
- Impactful effects of NP morphology, coating technique, and drying medium on corrosion resistance.
- The oven-dried Ag NPs and Cu NPs coated Ti6Al4V alloy by spray coating exhibited the best substrate protection with the highest OCP value.
- Correlation between small particle size, uniform distribution, low agglomeration, and smooth surfaces contributing to enhanced corrosion protection.
- The potential for further biomedical applications of Ti6Al4V alloy through NP-induced surface modification.
- Recognition of the imperative need for eco-friendly anti-corrosion nanocomposite coatings, urging a holistic approach to biometallic coating design and fabrication.

CRediT authorship contribution statement

Gizem Karabulut: Writing – review & editing, Writing – original draft, Methodology, Formal analysis. **Nuray Beköz Üllen:** Writing – review & editing, Writing – original draft, Supervision. **Selcan Karakuş:** Writing – review & editing, Writing – original draft, Supervision, Methodology, Formal analysis, Conceptualization. **Mustafa Ersoy:** Writing – original draft, Formal analysis.

Declaration of competing interest

The authors declare that they have no known competing financial interests or personal relationships that could have appeared to influence the work reported in this paper.

Acknowledgements

This study was funded by Scientific Research Projects Coordination Unit of Istanbul University-Cerrahpaşa. Project number: FYL-2021-35633.

References

[1] I. Demetrescu, C. Pirvu, V. Mitran, Effect of nano-topographical features of Ti/TiO_2 electrode surface on cell response and electrochemical stability in artificial saliva, Bioelectrochemistry 79 (2010) 122–129, https://doi.org/10.1016/J.BIOELECHEM.2010.02.001.
[2] P. Jiang, Y. Zhang, R. Hu, B. Shi, L. Zhang, Q. Huang, Y. Yang, P. Tang, C. Lin, Advanced surface engineering of titanium materials for biomedical applications: from static modification to dynamic responsive regulation, Bioact. Mater. 27 (2023) 15–57, https://doi.org/10.1016/J.BIOACTMAT.2023.03.006.
[3] F. Variola, J.H. Yi, L. Richert, J.D. Wuest, F. Rosei, A. Nanci, Tailoring the surface properties of Ti6Al4V by controlled chemical oxidation, Biomaterials 29 (2008) 1285–1298, https://doi.org/10.1016/J.BIOMATERIALS.2007.11.040.
[4] S. Qiu, J. Ji, W. Sun, J. Pei, J. He, Y. Li, J.J. Li, G. Wang, Recent advances in surface manipulation using micro-contact printing for biomedical applications, Smart Mater. Med. 2 (2021) 65–73, https://doi.org/10.1016/J.SMAIM.2020.12.002.
[5] F.A. Shah, P. Thomsen, A. Palmquist, Osseointegration and current interpretations of the bone-implant interface, Acta Biomater. 84 (2019) 1–15, https://doi.org/10.1016/J.ACTBIO.2018.11.018.
[6] S. Ferraris, A. Vitale, E. Bertone, S. Guastella, C. Cassinelli, J. Pan, S. Spriano, Multifunctional commercially pure titanium for the improvement of bone integration: multiscale topography, wettability, corrosion resistance and biological functionalization, Mater. Sci. Eng. C 60 (2016) 384–393, https://doi.org/10.1016/J.MSEC.2015.11.049.
[7] M. Textor, C. Sittig, V. Frauchiger, S. Tosatti, D.M. Brunette, Properties and Biological Significance of Natural Oxide Films on Titanium and Its Alloys, 2001, pp. 171–230, https://doi.org/10.1007/978-3-642-56486-4_7.
[8] S. Spriano, S. Ferraris, G. Pan, C. Cassinelli, E. Vernè, Multifunctional Titanium: Surface Modification Process and Biological Response, Doi:10.1142/S0219519415400011.15, 2015, https://doi.org/10.1142/S0219519415400011.
[9] S. Ferraris, S. Spriano, G. Pan, A. Venturello, C.L. Bianchi, R. Chiesa, M.G. Faga, G. Maina, E. Vernè, Surface modification of Ti–6Al–4V alloy for biomineralization and specific biological response: part I, inorganic modification, J. Mater. Sci. Mater. Med. 22 (3) (2011) 533–545, https://doi.org/10.1007/S10856-011-4246-2.
[10] M.P. Nikolova, M.S. Chavali, Metal oxide nanoparticles as biomedical materials, Biomimetics 5 (2020) 27, https://doi.org/10.3390/BIOMIMETICS5020027.
[11] G.S. Kaliaraj, T. Siva, A. Ramadoss, Surface functionalized bioceramics coated on metallic implants for biomedical and anticorrosion performance – a review, J. Mater. Chem. B 9 (2021) 9433–9460, https://doi.org/10.1039/D1TB01301G.
[12] L. He, D. Dai, L. Xie, Y. Chen, C. Zhang, Biological effects, applications and strategies of nanomodification of dental metal surfaces, Mater. Des. 207 (2021) 109890, https://doi.org/10.1016/J.MATDES.2021.109890.
[13] K. Jeeva Jothi, S. Balachandran, K. Palanivelu, Synergistic combination of *Phyllanthus niruri*/silver nanoparticles for anticorrosive application, Mater. Chem. Phys. 279 (2022) 125794, https://doi.org/10.1016/J.MATCHEMPHYS.2022.125794.
[14] S. Jain, M.S. Mehata, Medicinal plant leaf extract and pure flavonoid mediated green synthesis of silver nanoparticles and their enhanced antibacterial property, Sci. Rep. 7 (2017) 1–13, https://doi.org/10.1038/s41598-017-15724-8.
[15] M. Venkatesham, D. Ayodhya, A. Madhusudhan, N. Veera Babu, G. Veerabhadram, A novel green one-step synthesis of silver nanoparticles using chitosan: catalytic activity and antimicrobial studies, Appl. Nanosci. 4 (2014) 113–119, https://doi.org/10.1007/S13204-012-0180-Y.

[16] G. Karabulut, N. Beköz Üllen, E. Akyüz, S. Karakuş, Surface modification of 316L stainless steel with multifunctional locust gum/polyethylene glycol-silver nanoparticles using different coating methods, Prog. Org. Coat. 174 (2023) 107291, https://doi.org/10.1016/J.PORGCOAT.2022.107291.

[17] T. Koutouzis, Implant-abutment connection as contributing factor to peri-implant diseases, Periodontol 2000 (81) (2019) 152–166, https://doi.org/10.1111/PRD.12289.

[18] Z. Li, J. Qiu, L.Q. Du, L. Jia, H. Liu, S. Ge, TiO_2 nanorod arrays modified Ti substrates promote the adhesion, proliferation and osteogenic differentiation of human periodontal ligament stem cells, Mater. Sci. Eng. C 76 (2017) 684–691, https://doi.org/10.1016/J.MSEC.2017.03.148.

[19] A.R. Grayeli-Korpi, H. Savaloni, Effect of nitrogen ion implantation on corrosion inhibition of nickel coated 316 stainless steel and correlation with nano-structure, Appl. Surf. Sci. 258 (2012) 9982–9988, https://doi.org/10.1016/J.APSUSC.2012.06.060.

[20] W. Shao, Q. Zhao, Effect of corrosion rate and surface energy of silver coatings on bacterial adhesion, Colloids Surf. B: Biointerfaces 76 (2010) 98–103, https://doi.org/10.1016/J.COLSURFB.2009.10.018.

[21] C.T. Kwok, F.T. Cheng, H.C. Man, W.H. Ding, Corrosion characteristics of nanostructured layer on 316L stainless steel fabricated by cavitation-annealing, Mater. Lett. 60 (2006) 2419–2422, https://doi.org/10.1016/J.MATLET.2006.01.053.

[22] F.W. Abdulsada, A.S. Hammood, Characterization of corrosion and antibacterial resistance of hydroxyapatite/silver nano particles powder on 2507 duplex stainless steel, Mater. Today Proc. 42 (2021) 2301–2307, https://doi.org/10.1016/J.MATPR.2020.12.319.

[23] H. Qian, M. Li, Z. Li, Y. Lou, L. Huang, D. Zhang, D. Xu, C. Du, L. Lu, J. Gao, Mussel-inspired superhydrophobic surfaces with enhanced corrosion resistance and dual-action antibacterial properties, Mater. Sci. Eng. C 80 (2017) 566–577, https://doi.org/10.1016/J.MSEC.2017.07.002.

[24] S. Tavakoli, S. Nemati, M. Kharaziha, S. Akbari-Alavijeh, Embedding CuO nanoparticles in PDMS-SiO_2 coating to improve antibacterial characteristic and corrosion resistance, Colloid Interface Sci. Commun. 28 (2019) 20–28, https://doi.org/10.1016/J.COLCOM.2018.11.002.

[25] D. Roe, B. Karandikar, N. Bonn-Savage, B. Gibbins, J. Baptiste Roullet, Antimicrobial surface functionalization of plastic catheters by silver nanoparticles, J. Antimicrob. Chemother. 61 (2008) 869–876, https://doi.org/10.1093/JAC/DKN034.

[26] X. Ye, L. Wang, Z.T.H. Tse, G. Tang, G. Song, Retraction notice to "Effects of high-energy electro-pulsing treatment on microstructure, mechanical properties and corrosion behavior of Ti–6Al–4V alloy" [MSEC Volume 49, Year 2015, Pages 851–860], Mater. Sci. Eng. C 90 (2018) 781, https://doi.org/10.1016/J.MSEC.2018.05.072.

[27] G. Karabulut, N. Beköz Üllen, S. Karakuş, C. Toruntay, Enhancing antibacterial and anticorrosive properties of 316L stainless steel with nanocoating of copper oxide nanoparticles, Mater. Chem. Phys. 308 (2023) 128265, https://doi.org/10.1016/J.MATCHEM-PHYS.2023.128265.

[28] J.D. Chelaru, L.M. Muresan, 2-Mercapto-5-acetylamino-1,3,4-thiadiazole as corrosion inhibitor for a naturally patinated monumental bronze artifact, Stud. Univ. Babeş-Bolyai. Chem. 59 (2014) 91–102.

[29] S. Rajeshkumar, L.V. Bharath, Mechanism of plant-mediated synthesis of silver nanoparticles – a review on biomolecules involved, characterisation and antibacterial activity, Chem. Biol. Interact. 273 (2017) 219–227, https://doi.org/10.1016/j.cbi.2017.06.019.

[30] I. Khan, K. Saeed, I. Khan, Nanoparticles: properties, applications and toxicities, Arab. J. Chem. 12 (2019) 908–931, https://doi.org/10.1016/J.ARABJC.2017.05.011.

[31] F. Gulbagca, S. Ozdemir, M. Gulcan, F. Sen, Synthesis and characterization of *Rosa canina*-mediated biogenic silver nanoparticles for anti-oxidant, antibacterial, antifungal, and DNA cleavage activities, Heliyon 5 (2019) e02980, https://doi.org/10.1016/J.HELIYON.2019.E02980.

[32] S.K. Das, S. Behera, J.K. Patra, H. Thatoi, Green synthesis of sliver nanoparticles using *Avicennia officinalis* and *Xylocarpus granatum* extracts and in vitro evaluation of antioxidant, antidiabetic and anti-inflammatory activities, J. Clust. Sci. 30 (2019) 1103–1113, https://doi.org/10.1007/S10876-019-01571-2.

[33] A. Santhosh, V. Theertha, P. Prakash, S. Smitha Chandran, From waste to a value added product: green synthesis of silver nanoparticles from onion peels together with its diverse applications, Mater. Today Proc. 46 (2021) 4460–4463, https://doi.org/10.1016/J.MATPR.2020.09.680.

[34] F. Parveen, B. Sannakki, M.V. Mandke, H.M. Pathan, Copper nanoparticles: synthesis methods and its light harvesting performance, Sol. Energy Mater. Sol. Cells 144 (2016) 371–382, https://doi.org/10.1016/J.SOLMAT.2015.08.033.

[35] E.S. Al-Sheddi, N.N. Farshori, M.M. Al-Oqail, S.M. Al-Massarani, Q. Saquib, R. Wahab, J. Musarrat, A.A. Al-Khedhairy, M.A. Siddiqui, Anticancer potential of green synthesized silver nanoparticles using extract of nepeta deflersiana against human cervical cancer cells (HeLA), Bioinorg. Chem. Appl. (Nov 2018) 9390784, https://doi.org/10.1155/2018/9390784.

[36] F. LewisOscar, C. Nithya, S. Vismaya, M. Arunkumar, A. Pugazhendhi, P. Nguyen-Tri, S.A. Alharbi, N.S. Alharbi, N. Thajuddin, In vitro analysis of green fabricated silver nanoparticles (AgNPs) against *Pseudomonas aeruginosa* PA14 biofilm formation, their application on urinary catheter, Prog. Org. Coat. 151 (2021) 106058, https://doi.org/10.1016/J.PORGCOAT.2020.106058.

[37] Z. Alhalili, Green synthesis of copper oxide nanoparticles CuO NPs from Eucalyptus Globoulus leaf extract: adsorption and design of experiments, Arab. J. Chem. 15 (2022) 103739, https://doi.org/10.1016/J.ARABJC.2022.103739.

[38] N.L.N. Trang, V.T. Hoang, N.X. Dinh, L.T. Tam, V.P. Le, D.T. Linh, D.M. Cuong, N. T. Khi, N.H. Anh, P.T. Nhung, A.T. Le, Novel eco-friendly synthesis of biosilver nanoparticles as a colorimetric probe for highly selective detection of Fe (III) ions in aqueous solution, J. Nanomater. 2021 (2021), https://doi.org/10.1155/2021/5527519.

[39] M. Soloviev, A. Gedanken, Coating a stainless steel plate with silver nanoparticles by the sonochemical method, Ultrason. Sonochem. 18 (2011) 356–362, https://doi.org/10.1016/J.ULTSONCH.2010.06.015.

[40] R. Alias, R. Mahmoodian, M.H. Abd Shukor, Development and characterization of a multilayer silver/silver-tantalum oxide thin film coating on stainless steel for biomedical applications, Int. J. Adhes. Adhes. 92 (2019) 89–98, https://doi.org/10.1016/J.IJADHADH.2019.04.010.

[41] S. Zhang, X. Liang, G.M. Gadd, Q. Zhao, A sol–gel based silver nanoparticle/polytetrafluorethylene (AgNP/PTFE) coating with enhanced antibacterial and anti-corrosive properties, Appl. Surf. Sci. 535 (2021) 147675, https://doi.org/10.1016/J.APSUSC.2020.147675.

[42] I.A. Aminatun, D. Furqon, C.A.C. Hikmawati, Abdullah, antibacterial properties of silver nanoparticle (AgNPs) on stainless steel 316L, Nanomed. Res. J. 6 (2021) 117–127, https://doi.org/10.22034/NMRJ.2021.02.004.

[43] V. Milleret, P.S. Lienemann, A. Gasser, S. Bauer, M. Ehrbar, A. Wennerberg, Rational design and in vitro characterization of novel dental implant and abutment surfaces for balancing clinical and biological needs, Clin. Implant. Dent. Relat. Res. 21 (2019) 15–24, https://doi.org/10.1111/CID.12736.

[44] Y. Zhang, K. Gulati, Z. Li, P. Di, Y. Liu, K. Zhang, Z. Gulati, P. Li, Y. Liu Di, E. Ivanova, Dental implant nano-engineering: advances, limitations and future directions, Nanomaterials 11 (2021) 2489, https://doi.org/10.3390/NANO11102489.

[45] M. Geetha, A.K. Singh, R. Asokamani, A.K. Gogia, Ti based biomaterials, the ultimate choice for orthopaedic implants – a review, Prog. Mater. Sci. 54 (2009) 397–425, https://doi.org/10.1016/J.PMATSCI.2008.06.004.

[46] N. Beköz Üllen, G. Karabulut, S. Karakuş, Assessing the surface properties of plant extract-based silver nanoparticle coatings on 17–4 PH stainless steel foams using artificial intelligence-supported RGB analysis: a comparative study, J. Mater. Eng. Perform. (2023) 1–18, https://doi.org/10.1007/S11665-023-08322-5.

[47] T. Albrektsson, A. Wennerberg, On osseointegration in relation to implant surfaces, Clin. Implant. Dent. Relat. Res. 21 (2019) 4–7, https://doi.org/10.1111/CID.12742.

[48] S. Theimer, M. Graunitz, M. Schulze, F. Gaertner, T. Klassen, Optimization adhesion in cold spraying onto hard substrates: a case study for brass coatings, J. Therm. Spray Technol. 28 (2019) 124–134, https://doi.org/10.1007/S11666-018-0821-0.

[49] Y. Fu, F. Zhou, J. Feng, H. Luo, M. Zhang, Long-term corrosion resistance and friction-induced antibacterial enhancement of CrMoSiCN coating on Ti6Al4V alloy, Corros. Sci. 186 (2021) 109478, https://doi.org/10.1016/J.CORSCI.2021.109478.

[50] T. Liu, H. Zhao, J. Li, D. Zhang, W. Zheng, L. Wang, POSS-tetraaniline based giant molecule: synthesis, self-assembly, and active corrosion protection of epoxy-based organic coatings, Corros. Sci. 168 (2020) 108555, https://doi.org/10.1016/J.CORSCI.2020.108555.

[51] F. Bir, H. Khireddine, Z. Mekhalif, S. Bonnamy, Pulsed electrodeposition of Ag+ doped prosthetic Fluorohydroxyapatite coatings on stainless steel substrates, Mater. Sci. Eng. C 118 (2021) 111325, https://doi.org/10.1016/J.MSEC.2020.111325.

[52] A.M. Echavarría, J.A. Calderón, G. Gilberto Bejarano, Characterization of the structure and electrochemical behavior of Ag-TaN nanostructured composite coating for biomedical applications, Surf. Coat. Technol. 345 (2018) 1–12, https://doi.org/10.1016/J.SURFCOAT.2018.04.012.

[53] J. Kuang, Z. Ba, Z. Li, Z. Wang, J. Qiu, The study on corrosion resistance of superhydrophobic coatings on magnesium, Appl. Surf. Sci. 501 (2020) 144137, https://doi.org/10.1016/J.APSUSC.2019.144137.

[54] X. Zhang, Y. Yu, D. Jiang, Y. Jiao, Y. Wu, Z. Peng, J. Zhou, J. Wu, Z. Dong, Synthesis and characterization of a bi-functional hydroxyapatite/Cu-doped TiO_2 composite coating, Ceram. Int. 45 (2019) 6693–6701, https://doi.org/10.1016/J.CERAMINT.2018.12.158.

[55] D. Devadoss, A. Asirvatham, A. Kujur, G. Saaron, N. Devi, S. John Mary, Green synthesis of copper oxide nanoparticles from *Murraya koenigii* and its corrosion resistivity on Ti-6Al-4V dental alloy, J. Mech. Behav. Biomed. Mater. 146 (2023) 106080, https://doi.org/10.1016/J.JMBBM.2023.106080.

[56] D. Ionita, C. Ungureanu, I. Demetrescu, Electrochemical and antibacterial performance of CoCrMo alloy coated with hydroxyapatite or silver nanoparticles, J. Mater. Eng. Perform. 22 (2013) 3584–3591, https://doi.org/10.1007/S11665-013-0653-5/TABLES/3.

[57] D. Ionita, M. Grecu, C. Ungureanu, I. Demetrescu, Modifying the TiAlZr biomaterial surface with coating, for a better anticorrosive and antibacterial performance, Appl. Surf. Sci. 257 (2011) 9164–9168, https://doi.org/10.1016/J.APSUSC.2011.05.125.

[58] S. Höhn, S. Virtanen, Biocorrosion of TiO_2 nanoparticle coating of Ti–6Al–4V in DMEM under specific in vitro conditions, Appl. Surf. Sci. 329 (2015) 356–362, https://doi.org/10.1016/J.APSUSC.2014.12.114.

[59] N. Zaveri, G.D. McEwen, R. Karpagavalli, A. Zhou, Biocorrosion studies of TiO_2 nanoparticle-coated Ti-6Al-4V implant in simulated biofluids, J. Nanopart. Res. 12 (2010) 1609–1623, https://doi.org/10.1007/S11051-009-9699-6/FIGURES/10.

[60] C. García-Cabezón, V. Godinho, C. Salvo-Comino, Y. Torres, F. Martín-Pedrosa, Improved corrosion behavior and biocompatibility of porous titanium samples coated with bioactive chitosan-based nanocomposites, Materials 14 (2021) 6322, https://doi.org/10.3390/MA14216322.

[61] M.A. Massa, C. Covarrubias, M. Bittner, I.A. Fuentevilla, P. Capetillo, A. Von Marttens, J.C. Carvajal, Synthesis of new antibacterial composite coating for titanium based on highly ordered nanoporous silica and silver nanoparticles, Mater. Sci. Eng. C 45 (2014) 146–153, https://doi.org/10.1016/j.msec.2014.08.057.

[62] E. De Giglio, D. Cafagna, S. Cometa, A. Allegretta, A. Pedico, L.C. Giannossa, L. Sabbatini, M. Mattioli-Belmonte, R. Iatta, An innovative, easily fabricated, silver nanoparticle-based titanium implant coating: development and analytical characterization, Anal. Bioanal. Chem. 405 (2013) 805–816, https://doi.org/10.1007/s00216-012-6293-z.

[63] H. Líbalová, P.M. Costa, M. Olsson, L. Farcal, S. Ortelli, M. Blosi, J. Topinka, A. L. Costa, B. Fadeel, Toxicity of surface-modified copper oxide nanoparticles in a mouse macrophage cell line: interplay of particles, surface coating and particle dissolution, Chemosphere 196 (2018) 482–493, https://doi.org/10.1016/J.CHEMOSPHERE.2017.12.182.